



# Photochromic Fluorophores Enable Imaging of Lowly Expressed Proteins in the Autofluorescent Fungus *Candida albicans*

 Wouter Van Genechten,<sup>a,b,c</sup>  Liesbeth Demuyser,<sup>a,b</sup>  Sam Duwé,<sup>c</sup> Wim Vandenberg,<sup>d</sup>  Patrick Van Dijck,<sup>a,b</sup>  
 Peter Dedecker<sup>d</sup>

<sup>a</sup>Laboratory of Molecular Cell Biology, Institute of Botany and Microbiology, KU Leuven, Leuven, Belgium

<sup>b</sup>VIB-KU Leuven Center for Microbiology, KU Leuven, Leuven, Belgium

<sup>c</sup>Advanced Optical Microscopy Centre, Biomedical Research Institute (BIOMED), Hasselt University, Hasselt, Belgium

<sup>d</sup>Lab for Nanobiology, Department of Chemistry, KU Leuven, Leuven, Belgium

**ABSTRACT** Fluorescence microscopy is a standard research tool in many fields, although collecting reliable images can be difficult in systems characterized by low expression levels and/or high background fluorescence. We present the combination of a photochromic fluorescent protein and stochastic optical fluctuation imaging (SOFI) to deliver suppression of the background fluorescence. This strategy makes it possible to resolve lowly or endogenously expressed proteins, as we demonstrate for Gcn5, a histone acetyltransferase required for complete virulence, and Erg11, the target of the azole antifungal agents in the fungal pathogen *Candida albicans*. We expect that our method can be readily used for sensitive fluorescence measurements in systems characterized by high background fluorescence.

**IMPORTANCE** Understanding the spatial and temporal organization of proteins of interest is key to unraveling cellular processes and identifying novel possible antifungal targets. Only a few therapeutic targets have been discovered in *Candida albicans*, and resistance mechanisms against these therapeutic agents are rapidly acquired. Fluorescence microscopy is a valuable tool to investigate molecular processes and assess the localization of possible antifungal targets. Unfortunately, fluorescence microscopy of *C. albicans* suffers from extensive autofluorescence. In this work, we present the use of a photochromic fluorescent protein and stochastic optical fluctuation imaging to enable the imaging of lowly expressed proteins in *C. albicans* through the suppression of autofluorescence. This method can be applied in *C. albicans* research or adapted for other fungal systems, allowing the visualization of intricate processes.

**KEYWORDS** *Candida albicans*, Erg11, Gcn5, fluorescence microscopy, photochromic fluorophores

Fluorescence imaging has contributed to many discoveries in a wide variety of systems. The microscopic imaging of fungi, for example, has led to a greater understanding of the virulence mechanisms in pathogens such as *Candida albicans*. This opportunistic fungal pathogen can cause bloodstream infections, also called candidemia, which has a crude mortality rate of approximately 40% (1). Fluorescence imaging of this organism has been performed on both a macroscale (2) and a subcellular scale, although both approaches tend to make use of the overexpression of specific targets labeled with a range of fluorescent proteins (FPs) (3–6).


Imaging of labeled molecules is often hampered by autofluorescence, which can originate from the presence of many weakly fluorescent molecules such as vitamin B<sub>2</sub> (7, 8). This vitamin, also termed riboflavin, is synthesized by *C. albicans* upon the activation of the protein kinase A (PKA) pathway (7). Its green-yellow emission is especially

**Citation** Van Genechten W, Demuyser L, Duwé S, Vandenberg W, Van Dijck P, Dedecker P. 2021. Photochromic fluorophores enable imaging of lowly expressed proteins in the autofluorescent fungus *Candida albicans*. mSphere 6:e00146-21. <https://doi.org/10.1128/mSphere.00146-21>.

**Editor** Aaron P. Mitchell, University of Georgia

**Copyright** © 2021 Van Genechten et al. This is an open-access article distributed under the terms of the [Creative Commons Attribution 4.0 International license](https://creativecommons.org/licenses/by/4.0/).

Address correspondence to Patrick Van Dijck, [patrick.vandijck@kuleuven.be](mailto:patrick.vandijck@kuleuven.be), or Peter Dedecker, [peter.dedecker@kuleuven.be](mailto:peter.dedecker@kuleuven.be).

 If you have a hard time visualizing your protein in *C. albicans*, find the solution in this new mSphere paper. @PatrickDijck

**Received** 25 February 2021

**Accepted** 27 February 2021

**Published** 17 March 2021

problematic when the labeled proteins are expressed at low levels, as is often the case for endogenous expression levels, especially because the brightest and best-maturing fluorescent proteins are typically located in this spectral region. Overexpression of fusion constructs is one way of improving the obtained signal but may interfere with the cellular phenotype (9) and can lead to accumulation in the endoplasmic reticulum (ER), vacuole, and terminal membranes (9).

These limitations pose challenges for many cellular targets. One example is Erg11, a cytochrome P450 (CYP) (10) and target of the first-line antifungal fluconazole (11). It is known that overexpression of CYPs can lead to ER stress (12), and visualization of Erg11 under endogenous expression is therefore important to correctly assess its localization. Previous experiments by our group showed the localization of Erg11 to the ER and plasma membrane in *Saccharomyces cerevisiae* under conditions of overexpression (13). Another example is Gcn5, a histone acetyltransferase involved in hypha formation and the cell wall stress response. Overexpression showed localization to the nucleus during the stationary phase and in the cytosol during the exponential phase (5), although imaging of Gcn5 under endogenous expression did not result in a usable signal.

Recently, we codon optimized fast-folding Dronpa (ffDronpa), a novel type of “smart” fluorescent protein, resulting in the CeffDronpa label for applications in *C. albicans* (4). The fluorescence emission of ffDronpa can be switched “on” and “off” using 405- and 488-nm light, respectively (14), enabling applications in diffraction-unlimited fluorescence imaging (15) using techniques such as photochromic stochastic optical fluctuation imaging (pcSOFI), photoactivated localization microscopy (PALM), or reversible saturable optical fluorescence transitions (RESOLFT) (16–18). pcSOFI relies on the acquisition of multiple fluorescence images (hundreds or more) from fluorophores that show fluorescence dynamics or “blinking.” Statistical analysis of the acquired images then leads to a superresolved image with a resolution enhancement of up to 2- or 3-fold or more (16, 19).

Since it relies on the analysis of single-molecule fluorescence fluctuations, pcSOFI is highly sensitive to the emission from bright emitters with pronounced intensity fluctuations, such as photochromic fluorescent proteins, but effectively insensitive to emission originating from a large number of weakly autofluorescent molecules, as is typically the case for background emitters.

Other reports have investigated the use of photochromic proteins to reduce background levels, although these approaches often require customization of the instrument so that it can generate specific illumination sequences with precise timing control (20–22). pcSOFI, in contrast, derives its enhancement from the spontaneous blinking of the fluorophores, which means that no adaptation or customization of the instrument is required.

In this contribution, we applied pcSOFI microscopy to samples labeled with CeffDronpa. We find that this strategy results in efficient background rejection and a more straightforward assessment of protein localization without interference of autofluorescence. We also demonstrate the imaging of lowly expressed targets, thereby increasing the set of proteins that can be visualized via labeling of the endogenous population. In particular, we show that Erg11 localizes to the ER and the plasma membrane in *C. albicans*, while a proportion of Gcn5 localizes to the nucleus and the cytosol depending on the growth phase. We expect that our approach can deliver enhanced imaging in a range of organisms.

## RESULTS AND DISCUSSION

**Background fluorescence in *C. albicans*.** We first sought to quantify the background fluorescence in *C. albicans* wild-type strain SC5314 relative to *S. cerevisiae* laboratory strain S288C. Flow cytometry measurements show a significant difference ( $P=0.003$ ) in the emission of the unlabeled cells, even though both strains have similar physical sizes as measured using the forward-scatter component. As shown in Fig. 1A,

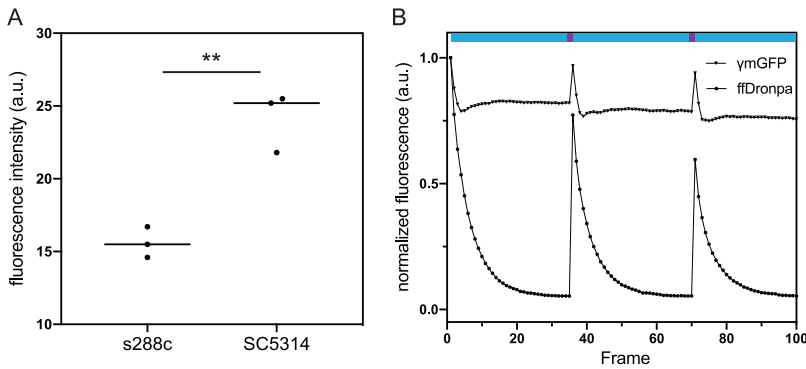


**FIG 1** (A) Autofluorescence of *S. cerevisiae* diploid strain S288C and *C. albicans* wild-type strain SC5314 measured using flow cytometry. Cells were grown overnight on LoFlo medium to the exponential phase (4 to 5 h) before measurement. Asterisks denote the significance level, with \*\* corresponding to a *P* value of  $<0.01$  as calculated using Student's *t* test. (B) *In vivo* photoswitching assessment of *C. albicans* overexpressing CeffDronpa or  $\gamma$ mGFP. Fluorescent proteins were cycled by exposing the cells to one pulse of 405-nm laser light (purple bars) to induce switching to the fluorescent state before capturing 35 images using 488-nm excitation (cyan bars). a.u., arbitrary units.

the background signal of *C. albicans* is almost 2-fold higher, indicating that fluorescence imaging of *C. albicans* in a similar spectral window is more challenging. This bright autofluorescence is omnipresent in filamentous fungi where lipofuscin, ergosterol, riboflavin, flavin adenine dinucleotide, and cell wall components significantly contribute to the background signal (7, 23–26).

***In vivo* reversible switching of *Candida*-enhanced ffDronpa.** We then verified whether CeffDronpa retains its photochromism in *C. albicans*. We overexpressed the protein and found that it is able to switch reversibly between the dark and the bright states, as indicated in Fig. 1B. The initial fluorescence of the cells is relatively high and drops quickly to a plateau approximately equal to the background fluorescence upon applying 488-nm illumination, resulting in a large contrast between the on- and off-states of the FP *in vivo*. A subsequent 405-nm pulse is able to recover the fluorescence to approximately 75% of the maximum fluorescence of the previous cycle, suggesting some photodestruction of the label. Thus, *in vivo*, CeffDronpa ( $pK_a$ , 5.0) displays robust photochromism, even though the cytosolic pH of *Candida albicans* ranges from 6 to 7, which is more acidic than the mammalian cytosolic pH of 7.1 to 7.2 (27). We also included  $\gamma$  monomeric green fluorescent protein ( $\gamma$ mGFP) expressing cells as a reference. We find that the resulting cells show  $\pm 25\%$  higher fluorescence brightness but do not show the pronounced modulation pattern displayed by cells expressing CeffDronpa.

**Localization of Gcn5 to the nucleus and the cytosol.** Gcn5 is a catalytic subunit of the histone acetyltransferase complex SAGA, which is involved in one of the main virulence factors of *C. albicans*. Deletion of *GCN5* rendered *C. albicans* nonvirulent in a mouse tail vein infection model (5). Imaging of a Gcn5-GFP fusion construct under constitutive expression from the *ADH1* promoter (overexpression) showed nuclear localization in the stationary growth phase and cytoplasmic localization in the exponential growth phase (5). However, no signal was observed from the expression of the fusion construct under the control of the native promoter, rendering the localization of Gcn5 at endogenous levels uncertain (5).

We constructed a Gcn5-CeffDronpa fusion protein under the control of the endogenous promoter and visualized its expression in live cells. Figure 2 shows the averaged (non-pcSOFI) signal from the green channel as well as an overlay with the NucBlue nuclear marker. This averaged image was obtained by combining the first 15 images in the SOFI image stack and can be considered to be a classical wide-field image of the same region of the same sample. The non-SOFI images (Fig. 2A and E) show some brighter features and a high degree of autofluorescence, comparable to images acquired on cells that did not express any fluorescent proteins (Fig. 2I and M). We

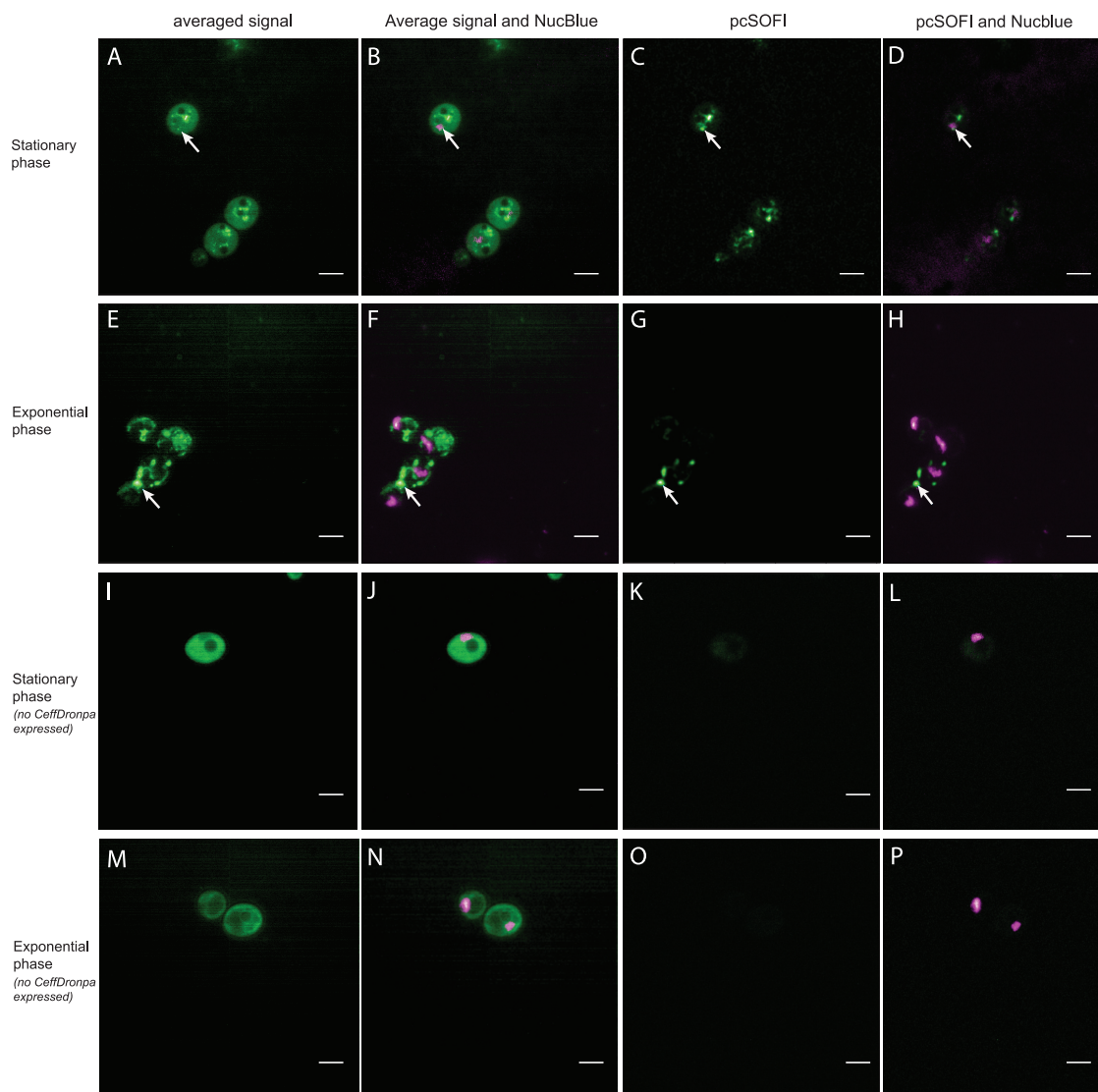


**FIG 2** (A to H) Imaging of Gcn5 tagged with CeffDronpa in the stationary phase (A to D) and the exponential phase (E to H) using pcSOFI. White arrows indicate points of interest in both the averaged wide-field and pcSOFI processed images. (A and E) Averaged images of a stack obtained in the green channel by exciting cells using 488-nm light. (B and F) Overlays of the averaged image, with the NucBlue staining in magenta. (C and G) pcSOFI postprocessing of the same stack. (D and H) Overlays of the resulting pcSOFI images, with NucBlue staining in magenta. (I to P) Imaging of the negative-control samples for the Gcn5-CeffDronpa measurements in the stationary phase (I to L) and the exponential phase (M to P). (I and M) Averaged images of a stack obtained in the green channel by exciting cells using 488-nm light. (J and N) Overlays of the averaged image, with NucBlue staining in magenta. (K and O) pcSOFI postprocessing of the same stack. (L and P) Overlays of the resulting pcSOFI images, with NucBlue staining in magenta. Bars, 5  $\mu$ m.

concluded that it is difficult to distinguish relevant features from the cellular autofluorescence, confirming the difficulty of observing Gcn5 at endogenous levels.

We then applied our pcSOFI analysis to these samples, leading to the images shown in Fig. 2C, D, G and H. Compared to conventional imaging, the pcSOFI images show more cellular structuring and features and do not show the unstructured background emission. Some of these features could be partially observed already by conventional imaging, although pcSOFI imaging improved the contrast (Fig. 2, white arrows). A representative data set is shown for both the stationary and exponential phase. Additional data sets of the biological replicates in each growth condition are available at Zenodo (<https://doi.org/10.5281/zenodo.4265989>).

During the stationary phase, a proportion of the signal obtained from the Gcn5 fusion appears to colocalize to the nucleus (Fig. 2D), while exponentially growing cells

show distinct structures without indications of an overlap of the nuclear staining (Fig. 2G and H). Negative-control images of cells stained with NucBlue but not expressing CeFFDronpa show autofluorescence in the average images but no pcSOFI signal in both the stationary and exponential phases (Fig. 2K and O). This shows that neither NucBlue staining nor cellular autofluorescence leads to the fluorescence dynamics detected by the pcSOFI signal.

**Localization of Erg11 to the ER and plasma membrane.** The most widely used class of antifungals, the azoles, targets the biosynthesis of ergosterol. More specifically, azoles target the lanosterol-14- $\alpha$ -demethylase enzyme encoded by *ERG11*. This key enzyme in the ergosterol biosynthesis pathway is therefore a frequently studied protein that can acquire multiple point mutations that confer resistance to azoles. In *S. cerevisiae*, it was shown to localize to both the endoplasmic reticulum and the plasma membrane via focused ion beam scanning electron microscopy (FIB SEM) (13). The extensive sequence similarity between *S. cerevisiae* Erg11 (ScErg11) and *C. albicans* Erg11 (CaErg11) suggests that a similar localization may occur in *C. albicans* (28).

Figure 3 shows images obtained for a fusion construct between Erg11 and CeFFDronpa expressed at endogenous levels, confirming the results from *S. cerevisiae* and the prediction for *C. albicans*. The averaged signal images (Fig. 3A and C) show no visible structuring on account of the autofluorescence, which drowns out the CeFFDronpa signal. In the pcSOFI processed images (Fig. 3B and D), clear localization to the ER, in the form of a distinct ring around the nucleus, and the plasma membrane is observed. The administration of fluconazole, which was shown to increase the autofluorescence background of SC5314 (see Fig. S1 in the supplemental material), did not appear to influence the pcSOFI imaging. No pcSOFI signal was observed in control strains not expressing CeFFDronpa (Fig. 3F). Data are available at Zenodo (<https://doi.org/10.5281/zenodo.4265989>).

These two examples show that the removal of the background autofluorescence and, thus, the increase in the signal-to-noise ratio (SNR) allow for the visualization of low-abundance targets in living cells. A disadvantage of the imaging is that it requires higher light doses associated with single-molecule detection and that the temporal resolution is decreased since multiple images must be acquired. We required 18 s to acquire a single pcSOFI image at the expression levels observed here, although this could be accelerated by lowering the number of collected frames and/or employing a shorter exposure time at the cost of the resulting SNR.

In conclusion, our work shows that the combination of photochromic fluorophores with pcSOFI allows the reduction of nonlabel emission in fluorescence microscopy without customization of the microscope. We demonstrated the potential of this approach by generating endogenous fusion constructs with CeFFDronpa and visualizing the resulting fluorescence distribution in *C. albicans*. We propose that this method is a valuable strategy for applications in other systems showing high autofluorescence levels.

## MATERIALS AND METHODS

**Strain construction.** For the endogenous tagging of Gcn5 and Erg11, we constructed a pFA6-based plasmid containing the codon-optimized ffDronpa, CeFFDronpa. From the CeFFDronpa gBlock (IDT), we amplified a Gibson insert using primers listed in Table S1 in the supplemental material. The pFA6 plasmid, containing a nourseothricin marker, was digested with PstI and SmaI before the insertion of CeFFDronpa. From this pFA6-CeFFDronpa plasmid, we created linear PCR fragments with 100-bp homologous overhangs for recombination with the 3' end of the *GCN5* or *ERG11* gene, without the stop codon, and the 5' start of its terminator. Between the *GCN5* or *ERG11* gene and the start of the FP, we included a linker sequence containing a triple repetition of glycine and alanine (GAGAGA). These linear fragments were transformed into the wild-type *C. albicans* strain SC5314. Genomic DNA was sequenced to confirm the correct integration of CeFFDronpa.

**Photoswitching assessment.** *Candida* enhanced ffDronpa- and  $\gamma$ mGFP-expressing strains that were used in the photoswitching assessment were reported previously (4) and grown overnight on low-fluorescence (LoFlo) medium containing 0.69% (wt/vol) yeast nitrogen base (without amino acids, folic acid, and riboflavin), 0.25% (wt/vol) ammonium sulfate, 0.079% (wt/vol) complete supplement mixture (CSM; MP Biomedicals), and 2% (wt/vol) glucose. The strains were brought to an optical density at 600 nm ( $OD_{600}$ ) of 0.2 in fresh low-fluorescence medium and grown to the exponential phase (4 to 5 h) before

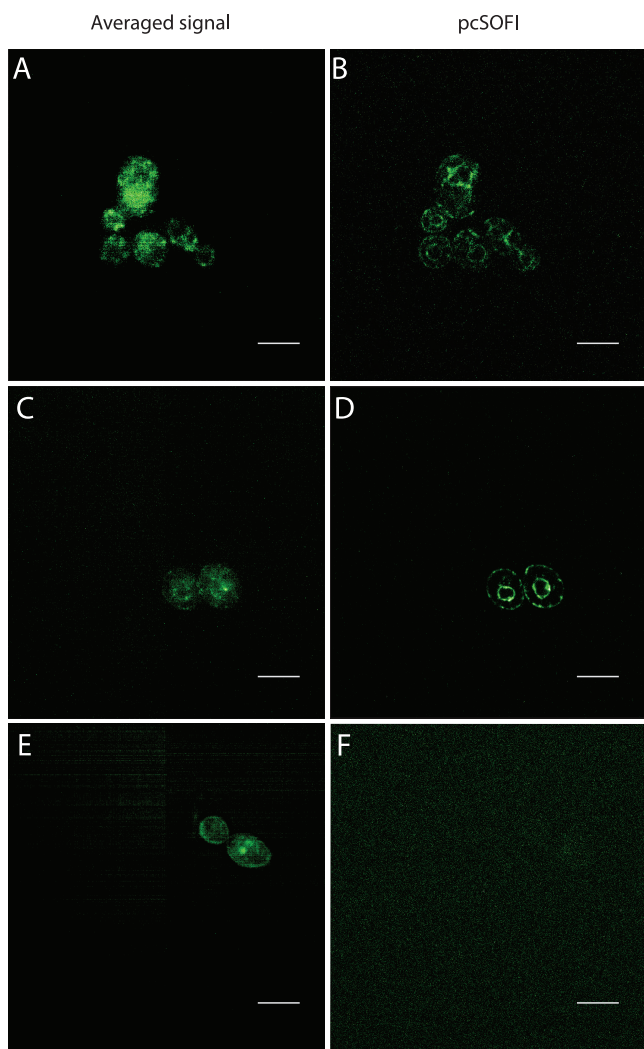


**FIG 3** Imaging of Erg11 tagged with CeFFDronpa. Cells were grown overnight on LoFlo medium to the exponential phase before measurement. (A and C) Averaged images of Erg11 tagged with CeFFDronpa to provide an indication of a wide-field image. (B and D) pcSOFI postprocessed images. (E) Averaged image of a negative-control sample. (F) pcSOFI postprocessed image of the negative-control sample. The slight striping visible in panels A, C, and E is due to the patterning of the scientific complementary metal-oxide semiconductor (sCMOS) camera, which becomes visible due to the low light levels, and is not a feature of the sample. Bars, 5  $\mu\text{m}$ .

measurement of photoswitching. The microscopic setup used for photoswitching and the following imaging experiments is a Nikon Ti2 epifluorescence microscope equipped with a Nikon 100 $\times$  CFI apo objective (numerical aperture [NA] = 1.49). Lasers used for photoswitching imaging are 405- and 488-nm Oxixius lasers. To assess the photoswitching capacity of *in vivo* CeFFDronpa, a cycle of on- and off-switching was induced, consisting of a 405-nm pulse followed by the acquisition of 35 images using 488-nm excitation and detection with a 540/30-nm-band-pass filter. Fluorescence images were collected with a Hamamatsu imageEM X2 instrument. The same measurement regime was applied to  $\gamma\text{mGFP}$ -expressing cells and wild-type SC5314. The fluorescence intensity of 10 cells for each strain was measured by manually selecting regions of interest (ROIs) and normalized to the first frame.

**Flow cytometry measurement of the background signal.** The background signals of three replicates of the *C. albicans* wild-type strain SC5314 and a diploid *Saccharomyces cerevisiae* strain, S288C, were measured using flow cytometry. Strains were grown overnight in yeast extract-peptone-dextrose (YPD) before bringing them to an optical density of 0.2. Cultures were grown for approximately 5 h in LoFlo medium in a 30 $^{\circ}\text{C}$  shaking incubator before measuring 100,000 cells with a BD influx flow cytometer with 488-nm excitation and a band-pass emission filter of 530/40 nm. The mean fluorescence intensity was calculated for each strain using FlowJo (29), and Student's *t* test was performed using GraphPad Prism.

**pcSOFI imaging. (i) Gcn5 imaging and pcSOFI processing.** The Gcn5 imaging experiment was carried out in a way to resemble the methods of the first publication reporting the localization of Gcn5 (5).

Cells were grown overnight in LoFlo medium until stationary phase. Part of this culture was diluted to an optical density of 0.2 in fresh LoFlo medium. These cells were grown for 4 to 5 h at 30°C until mid-exponential phase before staining the nucleus with NucBlue.

We first imaged NucBlue staining using excitation with 405-nm light and a 480/40-nm emission filter; subsequently, we acquired at least 1,500 frames of CeffDronpa-tagged Gcn5 using 488-nm excitation. Emission was recorded through a band-pass filter at 540/30 nm. To construct the SOFI image using the Localizer package in IgorPro (30), 600 frames were used, dropping the initial 15 frames to exclude non-stationary signals. The images produced were checked for artifacts using SOFIevaluator (31). Since the SNR of the images was limited, the image was subsequently convolved with a Gaussian function (full width at half-maximum [FWHM], 112.5 nm) to further smooth out the background noise and bring out the labeled features. Average images of frames 16 to 30 were also calculated to serve as an indication of the CeffDronpa abundance and background intensities.

**(ii) Erg11 imaging and pcSOFI processing.** For Erg11 imaging, cells were grown overnight in LoFlo medium until stationary phase before bringing this culture to an OD<sub>600</sub> of 0.2. To simulate experimental conditions under which research is performed within the susceptible-dose-dependent range of concentrations, we administered 16 µg/ml fluconazole to the culture (32, 33). Cells were grown at 30°C for 5 h before visualization using the same microscope setup as the one described above. The pcSOFI image analysis was performed using the Localizer package in IgorPro (30). The first 5 frames were not utilized in the reconstruction due to the initial nonstationary behavior. Frames 6 to 1,000 were utilized for the reconstruction. Average images of the first 15 frames were also calculated to serve as an indication of the CeffDronpa abundance and background intensities.

## SUPPLEMENTAL MATERIAL

Supplemental material is available online only.

**FIG S1**, EPS file, 0.3 MB.

**TABLE S1**, PDF file, 0.04 MB.

## ACKNOWLEDGMENTS

This work was supported by the Research Foundation Flanders (FWO Vlaanderen) (1S01817N to W.V.G. and G062616N to P.V.D. and P.D.) and ERC starting grant 714688 NanoCellActivity.

We thank Nico Vangoethem for the generous help in the creation of the figures.

We declare that there is no conflict of interest.

## REFERENCES

- Pfaller MA, Diekema DJ. 2007. Epidemiology of invasive candidiasis: a persistent public health problem. *Clin Microbiol Rev* 20:133–163. <https://doi.org/10.1128/CMR.00029-06>.
- Bergeron AC, Seman BG, Hammond JH, Archambault LS, Hogan DA, Wheeler RT. 2017. *Candida albicans* and *Pseudomonas aeruginosa* interact to enhance virulence of mucosal infection in transparent zebrafish. *Infect Immun* 85:e00475–17. <https://doi.org/10.1128/IAI.00475-17>.
- Gonia S, Berman J, Gale CA. 2017. Generation of fluorescent protein fusions in *Candida* species. *J Vis Exp* 2017:55333. <https://doi.org/10.3791/55333>.
- Van Genechten W, Demuyser L, Dedecker P, Van Dijck P. 2020. Presenting a codon-optimized palette of fluorescent proteins for use in *Candida albicans*. *Sci Rep* 10:6158. <https://doi.org/10.1038/s41598-020-63308-w>.
- Chang P, Fan X, Chen J. 2015. Function and subcellular localization of Gcn5, a histone acetyltransferase in *Candida albicans*. *Fungal Genet Biol* 81:132–141. <https://doi.org/10.1016/j.fgb.2015.01.011>.
- Rao KH, Ghosh S, Datta A. 2016. Env7p associates with the Golgin protein Imh1 at the trans-Golgi network in *Candida albicans*. *mSphere* 1:e00080-16. <https://doi.org/10.1128/mSphere.00080-16>.
- Demuyser L, Palmans I, Vandecruys P, Van Dijck P. 2020. Molecular elucidation of riboflavin production and regulation in *Candida albicans*, toward a novel antifungal drug target. *mSphere* 5:e00714-20. <https://doi.org/10.1128/mSphere.00714-20>.
- Graus MS, Neumann AK, Timlin JA. 2017. Hyperspectral fluorescence microscopy detects autofluorescent factors that can be exploited as a diagnostic method for *Candida* species differentiation. *J Biomed Opt* 22:16002. <https://doi.org/10.1117/1.JBO.22.1.016002>.
- Moore I, Murphy A. 2009. Validating the location of fluorescent protein fusions in the endomembrane system. *Plant Cell* 21:1632–1636. <https://doi.org/10.1105/tpc.109.068668>.
- Lepesheva GI, Waterman MR. 2004. CYP51—the omnipotent P450. *Mol Cell Endocrinol* 215:165–170. <https://doi.org/10.1016/j.mce.2003.11.016>.
- Ji H, Zhang W, Zhou Y, Zhang M, Zhu J, Song Y, Lu J. 2000. A three-dimensional model of lanosterol 14alpha-demethylase of *Candida albicans* and its interaction with azole antifungals. *J Med Chem* 43:2493–2505. <https://doi.org/10.1021/jm990589g>.
- Sandig G, Kargel E, Menzel R, Vogel F, Zimmer T, Schunck WH. 1999. Regulation of endoplasmic reticulum biogenesis in response to cytochrome P450 overproduction. *Drug Metab Rev* 31:393–410. <https://doi.org/10.1081/dmr-100101926>.
- Kerstens W, Kremer A, Holtappels M, Borghgraef P, Lippens S, Van Dijck P. 2020. Three-dimensional visualization of APEX2-tagged Erg11 in *Saccharomyces cerevisiae* using focused ion beam scanning electron microscopy. *mSphere* 5:e00981-19. <https://doi.org/10.1128/mSphere.00981-19>.
- Habuchi S, Ando R, Dedecker P, Verheijen W, Mizuno H, Miyawaki A, Hofkens J. 2005. Reversible single-molecule photoswitching in the GFP-like fluorescent protein Dronpa. *Proc Natl Acad Sci U S A* 102:9511–9516. <https://doi.org/10.1073/pnas.0500489102>.
- Dedecker P, De Schryver FC, Hofkens J. 2013. Fluorescent proteins: shine on, you crazy diamond. *J Am Chem Soc* 135:2387–2402. <https://doi.org/10.1021/ja309768d>.
- Dedecker P, Mo GC, Dertinger T, Zhang J. 2012. Widely accessible method for superresolution fluorescence imaging of living systems. *Proc Natl Acad Sci U S A* 109:10909–10914. <https://doi.org/10.1073/pnas.1204917109>.
- Flors C, Hotta J, Uji-i H, Dedecker P, Ando R, Mizuno H, Miyawaki A, Hofkens J. 2007. A stroboscopic approach for fast photoactivation-localization microscopy with Dronpa mutants. *J Am Chem Soc* 129:13970–13977. <https://doi.org/10.1021/ja074704l>.
- Dedecker P, Hotta J, Flors C, Sliwa M, Uji-i H, Roeflaers MB, Ando R, Mizuno H, Miyawaki A, Hofkens J. 2007. Subdiffraction imaging through the selective donut-mode depletion of thermally stable photoswitchable fluorophores: numerical analysis and application to the fluorescent

- protein Dronpa. *J Am Chem Soc* 129:16132–16141. <https://doi.org/10.1021/ja076128z>.
19. Dertinger T, Colyer R, Iyer G, Weiss S, Enderlein J. 2009. Fast, background-free, 3D super-resolution optical fluctuation imaging (SOFI). *Proc Natl Acad Sci U S A* 106:22287–22292. <https://doi.org/10.1073/pnas.0907866106>.
  20. Querard J, Zhang R, Kelemen Z, Plamont MA, Xie X, Chouket R, Roemgens I, Korepina Y, Albright S, Ipendey E, Volovitch M, Sladitschek HL, Neveu P, Gissot L, Gautier A, Faure JD, Croquette V, Le Saux T, Jullien L. 2017. Resonant out-of-phase fluorescence microscopy and remote imaging overcome spectral limitations. *Nat Commun* 8:969. <https://doi.org/10.1038/s41467-017-00847-3>.
  21. Abbandonato G, Storti B, Signore G, Beltram F, Bizzarri R. 2016. Quantitative optical lock-in detection for quantitative imaging of switchable and non-switchable components. *Microsc Res Tech* 79:929–937. <https://doi.org/10.1002/jemt.22724>.
  22. Marriott G, Mao S, Sakata T, Ran J, Jackson DK, Petchprayoon C, Gomez TJ, Warp E, Tulyathan O, Aaron HL, Isacoff EY, Yan Y. 2008. Optical lock-in detection imaging microscopy for contrast-enhanced imaging in living cells. *Proc Natl Acad Sci U S A* 105:17789–17794. <https://doi.org/10.1073/pnas.0808882105>.
  23. Dreyer B, Morte A, Pérez-Gilbert M, Honrubia M. 2006. Autofluorescence detection of arbuscular mycorrhizal fungal structures in palm roots: an underestimated experimental method. *Mycol Res* 110:887–897. <https://doi.org/10.1016/j.mycres.2006.05.011>.
  24. Knaus H, Blab G, van Veluw J, Gerritsen H, Wösten H. 2013. Label-free fluorescence microscopy in fungi. *Fungal Biol Rev* 27:60–66. <https://doi.org/10.1016/j.fbr.2013.05.003>.
  25. Ziegler S, Weiss E, Schmitt AL, Schlegel J, Burgert A, Terpitz U, Sauer M, Moretta L, Sivori S, Leonhardt I, Kurzai O, Einsele H, Loeffler J. 2017. CD56 is a pathogen recognition receptor on human natural killer cells. *Sci Rep* 7:6138. <https://doi.org/10.1038/s41598-017-06238-4>.
  26. Smail EH, Briza P, Panagos A, Berenfeld L. 1995. *Candida albicans* cell walls contain the fluorescent cross-linking amino acid dityrosine. *Infect Immun* 63:4078–4083. <https://doi.org/10.1128/IAI.63.10.4078-4083.1995>.
  27. Tournu H, Luna-Tapia A, Peters BM, Palmer GE. 2017. In vivo indicators of cytoplasmic, vacuolar, and extracellular pH using pHluorin2 in *Candida albicans*. *mSphere* 2:e00276-17. <https://doi.org/10.1128/mSphere.00276-17>.
  28. Skrzypek MS, Binkley J, Binkley G, Miyasato SR, Simison M, Sherlock G. 2017. The *Candida* Genome Database (CGD): incorporation of assembly 22, systematic identifiers and visualization of high throughput sequencing data. *Nucleic Acids Res* 45:D592–D596. <https://doi.org/10.1093/nar/gkw924>.
  29. Anonymous. 2019. FlowJo, vv10. Becton, Dickinson and Company, Ashland, OR.
  30. Dedecker P, Duwe S, Neely RK, Zhang J. 2012. Localizer: fast, accurate, open-source, and modular software package for superresolution microscopy. *J Biomed Opt* 17:126008. <https://doi.org/10.1117/1.JBO.17.12.126008>.
  31. Moeyaert B, Vandenberg W, Dedecker P. 2020. SOFlevaluator: a strategy for the quantitative quality assessment of SOFI data. *Biomed Opt Express* 11:636–648. <https://doi.org/10.1364/BOE.382278>.
  32. Demuyser L, Swinnen E, Fiori A, Herrera-Malaver B, Verstrepen K, Van Dijck P. 2017. Mitochondrial co-chaperone Mge1 is involved in regulating susceptibility to fluconazole in *Saccharomyces cerevisiae* and *Candida* species. *mBio* 8:e00201-17. <https://doi.org/10.1128/mBio.00201-17>.
  33. Pfaller MA, Diekema DJ, Sheehan DJ. 2006. Interpretive breakpoints for fluconazole and *Candida* revisited: a blueprint for the future of antifungal susceptibility testing. *Clin Microbiol Rev* 19:435–447. <https://doi.org/10.1128/CMR.19.2.435-447.2006>.